Zhou *et al. Energy Mater.* **2025**, *5*, 500033
DOI: 10.20517/energymater.2024.186

Energy Materials

Article

Open Access

A low-cost inorganic oxide as dual-functional electrolyte additive towards long cycling Li-rich Mn-based cathode materials

Dongwei Zhou[1], Guiyang Gao[1], Zhanlin Yang[2], Weibin Guo[4], Liang Lin[5], Yinggan Zhang[1,*], Chengkun Zhang[1], Saichao Li[1], Yuanyuan Liu[1], Baisheng Sa[2], Guoying Wei[3,*], Dong-Liang Peng[1], Jie Lin[1,*], Qingshui Xie[1,*]

[1]State Key Laboratory of Physical Chemistry of Solid Surface, Fujian Key Laboratory of Surface and Interface Engineering for High Performance Materials, College of Materials, Xiamen University, Xiamen 361005, Fujian, China.
[2]College of Materials Science and Engineering, Fuzhou University, Fuzhou 350108, Fujian, China.
[3]College of Materials & Chemistry, China Jiliang University, Hangzhou 310018, Zhejiang, China.
[4]Strait Institute of Flexible Electronics (SIFE, Future Technologies), Fujian Key Laboratory of Flexible Electronics, Fujian Normal University and Strait Laboratory of Flexible Electronics (SLoFE), Fuzhou 350117, Fujian, China.
[5]College of Physics and Energy, Fujian Normal University, Fuzhou 350117, Fujian, China.

***Correspondence to:** Yinggan Zhang, Senior Engineer, State Key Laboratory of Physical Chemistry of Solid Surface, Fujian Key Laboratory of Surface and Interface Engineering for High Performance Materials, College of Materials, Xiamen University, Siming South Road 422, Siming District, Xiamen 361005, Fujian, China. E-mail: ygzhang@xmu.edu.cn; Dr. Guoying Wei, College of Materials & Chemistry, China Jiliang University, Xueyuan Street 258, Qiantang District, Hangzhou 310018, Zhejiang, China. E-mail: guoyingwei@cjlu.edu.cn; Dr. Jie Lin, State Key Laboratory of Physical Chemistry of Solid Surface, Fujian Key Laboratory of Surface and Interface Engineering for High Performance Materials, College of Materials, Xiamen University, Siming South Road 422, Siming District, Xiamen 361005, Fujian, China. E-mail: linjie@xmu.edu.cn; Dr. Qingshui Xie, State Key Laboratory of Physical Chemistry of Solid Surface, Fujian Key Laboratory of Surface and Interface Engineering for High Performance Materials, College of Materials, Xiamen University, Siming South Road 422, Siming District, Xiamen 361005, Fujian, China. E-mail: xieqsh@xmu.edu.cn

How to cite this article: Zhou, D.; Gao, G.; Yang, Z.; Guo, W.; Lin, L.; Zhang, Y.; Zhang, C.; Li, S.; Liu, Y.; Sa, B.; Wei, G.; Peng, D. L.; Lin, J.; Xie, Q. A low-cost inorganic oxide as dual-functional electrolyte additive towards long cycling Li-rich Mn-based cathode materials. *Energy Mater.* **2025**, *5*, 500033. https://dx.doi.org/10.20517/energymater.2024.186

Received: 24 Sep 2024 **First Decision:** 18 Oct 2024 **Revised:** 26 Oct 2024 **Accepted:** 11 Nov 2024 **Published:** 23 Jan 2025

Academic Editor: Yuping Wu **Copy Editor:** Fangling Lan **Production Editor:** Fangling Lan

Abstract

Li-rich Mn-based cathode materials (LRM) have received great attention owing to their high capacity and low cost. However, the mismatch between the widely used carbonate electrolyte and the LRM cathode and lithium metal anode causes a series of problems, such as electrolyte continuous oxidation, cathode structure degradation, and Li dendritic growth. Herein, inorganic oxide B_2O_3 is introduced as a dual-functional high-voltage electrolyte additive to

construct stable cathode electrolyte interphase and solid electrolyte interphase for Li||LRM batteries. The modified interface derived from the additive can induce dendrite-free Li deposition, stabilize cathode structure, and inhibit transition metal dissolution. Moreover, the adverse side reactions are mitigated, thus enhancing Li^+ transport rate and reducing interface impedance. With the addition of B_2O_3 into the carbonate electrolyte, the Li||LRM battery exhibits an enhanced discharge capacity of 221 mAh g^{-1} after 200 cycles, equaling a capacity retention of 92.1%. When the upper cut-off voltage is increased to 5 V, a superior capacity retention of > 85% can still be achieved after 150 cycles at 1 C. In addition, the low cost of B_2O_3 benefits for commercial application. This work offers new guidance for the research of low-cost, high-voltage dual-functional additives for advanced lithium metal batteries.

Keywords: Li-rich Mn-based cathode, dual-functional additive, cathode electrolyte interphase, solid electrolyte interphase, carbonate electrolyte

INTRODUCTION

The rapid development of electric vehicles and portable electronic devices has brought great opportunities for the new energy industry while also raising the need to elevate the energy density of lithium (Li)-ion batteries[1,2]. In general, increasing the specific capacity of the active materials and operating voltage of the battery system are effective strategies to improve the battery energy density[3]. For anode materials, graphite, widely used in the commercial field, is unable to provide higher capacity. The lithium metal anode (LMA) with the highest specific capacity and lowest potential [3,860 mAh g^{-1}, 3.04 V *vs.* Standard Hydrogen Electrode (SHE)] has received widespread attention in recent years[4,5]. For cathode materials, the commonly used $LiFePO_4$ has a low specific capacity (~170 mAh g^{-1}), while high-nickel ternary cathode materials such as $LiNi_xCo_yMn_{1-x-y}O_2$ and $LiNi_xCo_yAl_{1-x-y}O_2$ ($x \geq 0.8$) have limited room for further specific capacity increase[6,7]. Among a series of cathode materials, Li-rich Mn-based layered oxides (LRM, $xLi_2MnO_3 \cdot (1-x)LiTMO_2$, where TM represents transition metal) have become a promising cathode due to the high specific capacity (> 250 mAh g^{-1}) and high energy density (> 1,000 Wh kg^{-1})[8-10]. Therefore, the Li|| LRM batteries provide a promising approach for high energy density lithium batteries.

However, for lithium-metal batteries, many interface issues between the electrodes and electrolytes need to be solved[11]. Firstly, the compatibility between LMA and conventional carbonate electrolytes is insufficient. The solid electrolyte interphase (SEI) formed in the initial cycle is difficult to inhibit the side reactions on the lithium metal surface, resulting in poor Coulombic efficiency (CE). Meanwhile, with the continuous and uneven plating/stripping of Li^+, it will induce the Li dendrites and dead Li, which significantly deteriorate the cycling life and safety of lithium-metal batteries[5,12]. In addition, for the LRM cathode, the lattice oxygen needs to be activated at a high voltage to participate in the redox reaction (> 4.5 V). However, when the voltage exceeds 4.3 V, the decomposition of carbonate electrolytes is intensified due to the low voltage tolerance, producing various harmful by-products[13]. These problems caused by electrolytes will eventually lead to low CE and continuous capacity attenuation of Li||LRM batteries, bringing great challenges to their practical application.

To improve the interfacial stability, various optimization strategies have been explored. For LMA, it is an available way to suppress Li dendrites by reducing local current density and volume change through three-dimensional skeleton structure[14-16]. Artificially creating lithiophilic SEI can also improve the uniformity of the deposited Li[17,18]. For comparison, constructing a functional SEI on the surface of LMA via electrolyte additives is a simple and effective method. Especially, the special components contained in the SEI (Li-N, Li-S-O species, *etc.*) can play an important role in inhibiting the generation of Li dendrites, inducing uniform Li deposition, and stabilizing the interfaces[19,20].

Apart from the LMA, building a passivation layer is also effective for cathode materials, but the conventional coatings are difficult to finely control, which may reduce the total capacity and increase the interface impedance[21-23]. Using highly concentrated electrolytes to reduce the proportion of free solvents is beneficial to mitigate solvent oxidation and construct the inorganic components of the cathode electrolyte interface (CEI), but it has inferior interface wettability and high cost[24]. By adding a small number of functional additives into the electrolyte, and then participating in the formation of CEI during cycling, the oxidative decomposition of the electrolyte can be effectively inhibited even under high-voltage conditions. Among the additives commonly used to modify the CEI, B-containing additives have garnered significant attention, including lithium bis(oxalate)borate (LiBOB)[25,26], $LiBF_4$ [3], lithium difluoro(oxalate)borate (LiDFOB)[27], *etc*. However, numerous studies have shown that the use of B-containing salts as additives can mitigate the electrolyte decomposition at high voltage, but they mainly enhance the performance of the cathode side without significantly influencing the LMA[3,25,28]. Moreover, high cost may also hinder their widespread application. Therefore, it is urgent to explore a low-cost additive that can improve both the performance of LMA and LRM cathodes under high voltage.

Given the positive effects of B-containing lithium salts on improving cycling performance, coupled with the low cost of oxides, B_2O_3 is regarded as a potential high-voltage additive. Herein, we introduce inorganic oxide B_2O_3 as a dual-function high-voltage additive. This additive can preferentially decompose on the surface of the LMA and LMR cathode, participating in the formation of CEI/SEI composed of B-containing species during the initial cycle, which can restrain the electrolyte decomposition on both electrodes. Furthermore, the formed CEI protective layer can hinder TM dissolution and help maintain the structural stability of LRM. A low-impedance SEI is also generated on the anode, which facilitates the migration of Li^+ and suppresses the growth of Li dendrites. Hence, through the combination of the modified CEI and SEI, this dual-functional additive can improve the overall electrochemical performance of Li||LRM batteries in a wide temperature range.

EXPERIMENTAL SECTION

Preparation of electrolytes and LRM cathodes

The electrolytes were prepared in a glove box filled with argon, and the concentrations of water and oxygen were controlled to be < 1 ppm. The blank electrolyte (BE) was purchased from Guangdong Canrd New Energy Technology Co., Ltd (China) and consisted of 1 M $LiPF_6$ dissolved in ethylene carbonate (EC): dimethyl carbonate (DMC): ethyl methyl carbonate (EMC) solvents (1:1:1, by weight). Then, B_2O_3 additives with different amounts of 0.25, 0.5, 1, and 1.5 wt% were introduced into the BE and denoted as B-0.25, B-0.5, B-1, and B-1.5, respectively. B_2O_3 was purchased from Acme-chem (China). LRM cathodes were synthesized by co-precipitation method using nickel sulfate, cobalt sulfate, and manganese sulfate as initial raw materials. Firstly, the precursor was prepared based on the molar ratio of Mn:Co:Ni = 4:1:1 with Na_2CO_3 as the precipitant, which was then pre-sintered at 500 °C to obtain the TM oxide. Finally, after uniformly mixing the TM oxide with $LiOH{\cdot}H_2O$, the mixtures were sintered at 800 °C to achieve the LRM cathode materials. An 80 wt% LRM, 10 wt% conductive agent (acetylene black) and 10 wt% binder [poly(vinylidene fluoride) (PVDF)] were dispersed into a certain amount of N-methyl-2-pyrrolidone (NMP) with stirring. Then, the collected slurry was cast onto the aluminum foil. After being dried overnight, the slurry-coated foil was punched into discs with a diameter of 12 mm. In detail, the mass loading of the cathode material was ~1.4 mg cm^{-2}, while the high mass loading was ~12.1 mg cm^{-2}.

Characterization

The cycled electrodes were disassembled from batteries, soaked in the DMC for approximately 6 h, and then dried naturally in the glove box for subsequent analyses. The surface morphologies of samples were observed by the scanning electron microscopy (SEM, Hitachi SU-70) and transmission electron microscope

(TEM, Talos F200). The crystal structure was analyzed by X-ray diffraction (XRD, Bruker-axs). Raman spectroscopy (Xplora) was employed to characterize the phase change. Surface chemical compositions were analyzed using X-ray photoelectron spectroscopy (XPS, PHI Quantum 2000) with a calibration of 284.8 eV for a C 1s peak. Quantitative analysis of dissolved TMs was performed using inductively coupled plasma mass spectrometry (ICP-MS, iCAP7400). Time-of-flight secondary ion mass spectrometry (TOF-SIMS 5, ION-TOF GmbH) was applied to detect the fragment information separated from the electrode surface.

Electrochemical measurements

The electrochemical tests were conducted in coin cells, where the separator was a Celgard 2500 microporous membrane. Linear sweep voltammetry (LSV) was performed in the electrochemical workstation (CHI660E, Shanghai Chenhua Instrument Corp), using stainless steel sheets as the working electrode, Li foil as both the counter electrode and reference electrode, with a scanning rate of 0.5 mV s^{-1}. Li||Cu batteries composed of copper foil, separators, Li foil, and electrolytes were used to evaluate the Li plating/stripping behavior. These batteries were first activated at 0.1 mA cm^{-2} for three cycles, followed by testing at 1 mA cm^{-2}. For polarization difference assessment, Li||Li symmetric batteries were employed, with Li foil as both the working electrode and counter electrode, at the current densities of 0.5, 1, and 2 mA cm^{-2}. The Tafel curves were obtained by testing the Li||Li symmetric batteries after ten cycles under a current density of 1 mA cm^{-2}, and the scanning rate was 0.1 mV s^{-1}. The assembled Li||LRM batteries were tested on the Neware battery testing system (CT-4008T, Neware Electronics Co., Ltd, China) to investigate the electrochemical properties. The initial activation rate was 0.2 C (1 C = 250 mAh g^{-1}), followed by the different rates at 2.0-4.8 V. For the tests with the upper cut-off voltage of 5 V, the first cycling voltage range was 2-4.8 V. The electrochemical impedance spectroscopy (EIS) investigation was carried out using the PARSTAT 3000A-DX electrochemical workstation (AMETEK Instrument Corp., USA), with a frequency range of 100,000-0.001 Hz and an amplitude voltage of 5 mV. The constant-voltage floating tests were recorded for 10 h at 4.8 V after 100 cycles at 1 C. The self-discharge tests were also obtained by charging to 4.8 V at 0.2 C after 50 and 100 cycles at 1 C. The galvanostatic intermittent titration technique (GITT) was applied to detect the Li^+ diffusion rate at 0.2 C for 20 min followed by a relaxation period of 3 h in the voltage range of 2.0-4.8 V. High and low temperature tests were evaluated under the conditions of 55 °C at 1 C and -15 °C at 0.33 C, respectively. Moreover, the *in-situ* XRD tests were carried out by assembling the cathode, separator, and lithium metal in a customized mold, and then connected with the XRD equipment to build the testing system. Subsequently, the changes of the (003) diffraction peak in the range of 17.5-19.5° were recorded during the initial two cycles at 0.5 C.

RESULTS AND DISCUSSION

Characterization of the electrolytes

To observe the dispersion state of the additive, 0.5 wt% of B_2O_3 was added into the BE, and then left to stand for one day. The results indicate that the electrolyte remains clear and transparent, with no visible deposits [Supplementary Figure 1]. The BE and B-0.5 electrolytes were irradiated by laser beams to identify the optical path in the solutions. It can be seen that no obvious laser beam appears in BE [Figure 1A]. However, when the upper, middle, and lower parts of B-0.5 are irradiated, the path of the beam passing through the solution can be clearly observed [Figure 1B-D]. This Tyndall phenomenon suggests that the additive is not dissolved in the electrolyte, but rather uniformly dispersed in the form of fine particles. Its insolubility in carbonate electrolytes is related to the covalent properties between B and O atoms.

LSV was conducted to verify the redox behavior of the electrolyte containing B_2O_3 at a scanning rate of 0.5 mV s^{-1}. Compared to BE, the oxidation current of B-0.5 increases significantly after 3.3 V in Figure 1E, corresponding to the preferential oxidation of B_2O_3 on the cathode surface, which facilitates the CEI formation. As shown in Figure 1F, there are two reduction peaks around 1.5 and 0.65 V in BE, which are

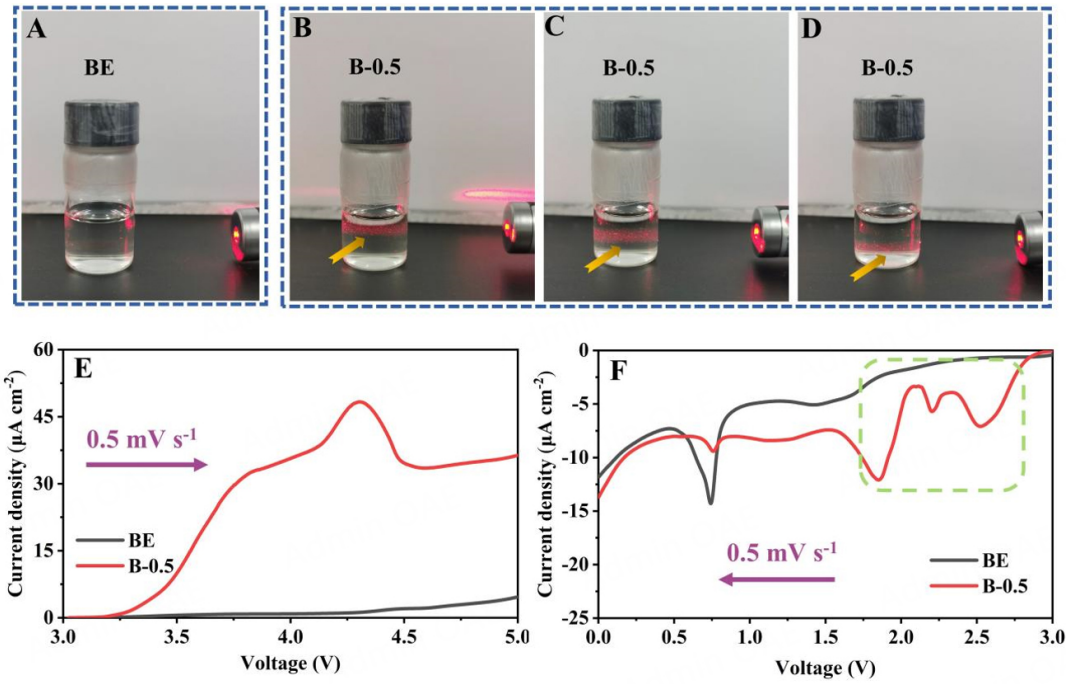

Figure 1. (A) Optical photos of the laser beam passing through BE. (B-D) Laser beam passing through (B) upper, (C) middle and (D) lower parts of B-0.5. (E) Oxidation and (F) reduction stability of BE and B-0.5 by LSV at a scan rate of 0.5 mV s^{-1}.

derived from the reduction reactions of linear and cyclic carbonate solvents in the electrolyte[20,21,29]. However, there are three evident peaks observed between 1.8 and 2.6 V in B-0.5. This may be attributed to the initial reduction reaction that occurs in B-0.5 generating unstable intermediates, which subsequently undergo further reactions as the voltage changes, ultimately forming the unique substances including Li-B-O species. Additionally, the intensity of reduction peak around 0.65 V is noticeably weakened in B-0.5. The findings suggest that B_2O_3 can also be preferentially reduced on the anode surface, which benefits the SEI formation and alleviates the decomposition of solvents. Therefore, the unique redox reactions provide the possibility for the additive to simultaneously improve the interfaces of both the cathode and anode sides.

Plating/Stripping behavior of Li metal

Symmetric cells are usually used to verify the cycling performance of LMA[15]. Herein, Li||Li symmetric cells were assembled and cycled at different current densities to evaluate the polarization behavior during Li plating/stripping processes. As shown in Figure 2A-D and Supplementary Figure 2, the polarization potential of the cells with BE exhibits a clear increase after 250 h at 0.5 mA cm^{-2} and 90 h at 1 mA cm^{-2}, respectively. Differently, at the same test conditions, the symmetric cells with B-0.5 still maintain stable and reduced overpotential after long-term cycling. In addition, there is a slightly higher overpotential of both samples in the initial stage, which remains stable after a period of cycling. This phenomenon is closely related to the original state of the lithium metal and the subsequent SEI formation[20]. Furthermore, when the current density is increased to 2 mA cm^{-2}, the cell with B-0.5 still exhibits better cycling performance than that with BE [Supplementary Figure 2A and B]. The polarization voltages after 50 and 100 h at different current densities are compared and shown in Supplementary Figure 2C and D. As the current density increases, the polarization gap between the two electrolytes also becomes larger. The above improvement effects are related to the high-quality SEI derived from B-0.5 (further analyzed in the subsequent sections), which is beneficial for accelerating the rapid migration of Li^+ at the interface. As a result, the compatibility between the electrolyte and LMA is enhanced.

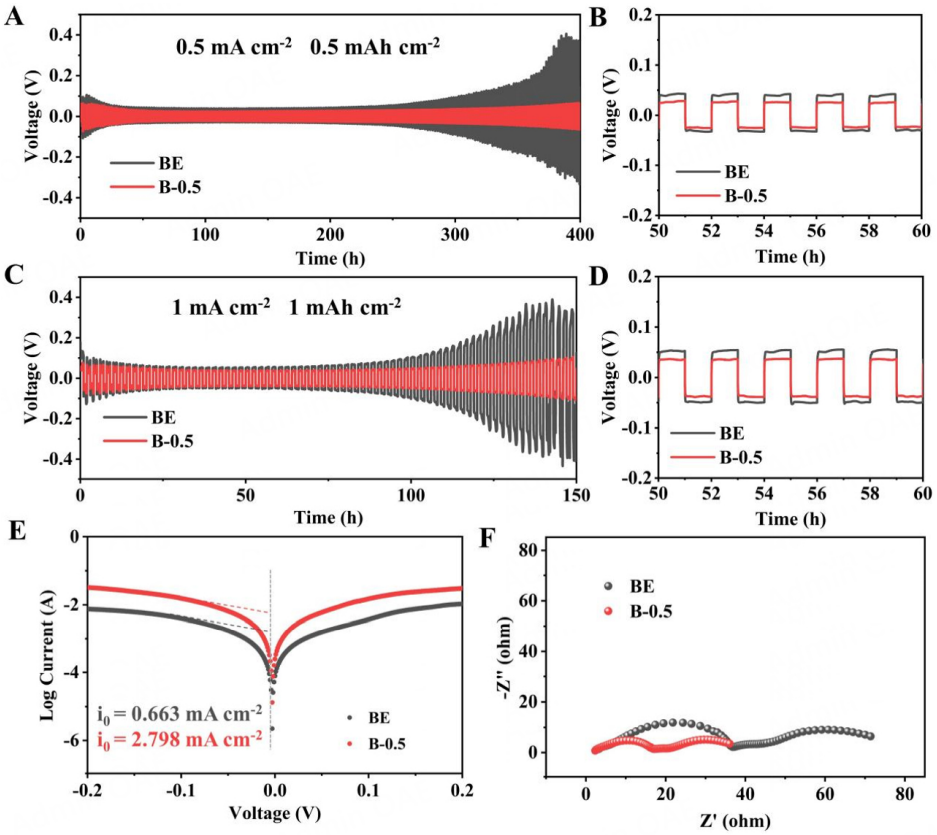

Figure 2. (A-D) Cycling performance of Li||Li symmetric cells at different current densities: (A and B) 0.5 mA cm^{-2} and 0.5 mAh cm^{-2}, (C and D) 1 mA cm^{-2} and 1 mAh cm^{-2}. (E) Tafel plots of Li||Li symmetric cells in different electrolytes. (F) Nyquist plot for Li||Li symmetric cells after ten cycles at 1 mA cm^{-2} and 1 mAh cm^{-2}.

The exchange current density and EIS were tested to understand the differences of SEI layers formed in BE and B-0.5. According to the test results of Li||Li symmetric cells after ten cycles, the exchange current density with B-0.5 is four times larger than that of BE, as shown in Figure 2E, revealing the enhanced reaction kinetics at the Li electrode/electrolyte interface in B-0.5. The rapid charge transfer ability helps suppress the uneven plating and uncontrollable dendritic growth of lithium metal. EIS tests also confirm that the additive is beneficial for reducing the interface impedance due to the highly conductive SEI layer [Figure 2F]. Therefore, the cells in B-0.5 show better rate performance than the BE, as presented in Supplementary Figure 3.

Li||Cu cells were used to further evaluate CE during the Li plating/stripping process. As presented in Supplementary Figure 4 and Figure 3A and B, at the conditions of 1 mA cm^{-2} and 1 mAh cm^{-2}, it can be seen that the CE of Li||Cu cell with B-0.5 is obviously higher than that with BE after 50 cycles. Moreover, the nucleation overpotential decreases from 283 to 179 mV after adding B_2O_3, as shown in Supplementary Figure 5, and the polarization potential at different cycles is also lower than that in BE [Figure 3C].

Besides, the deposition morphology of lithium metal in the two electrolytes was investigated using SEM. The lithium metal deposited on the Cu substrate appears to be loose and porous with severe dendritic growth in the BE electrolyte, as shown in Figure 3D, which accounts for the poor cycling performance and low CE. In comparison, a denser and flatter plating surface without obvious Li dendrites is obtained when

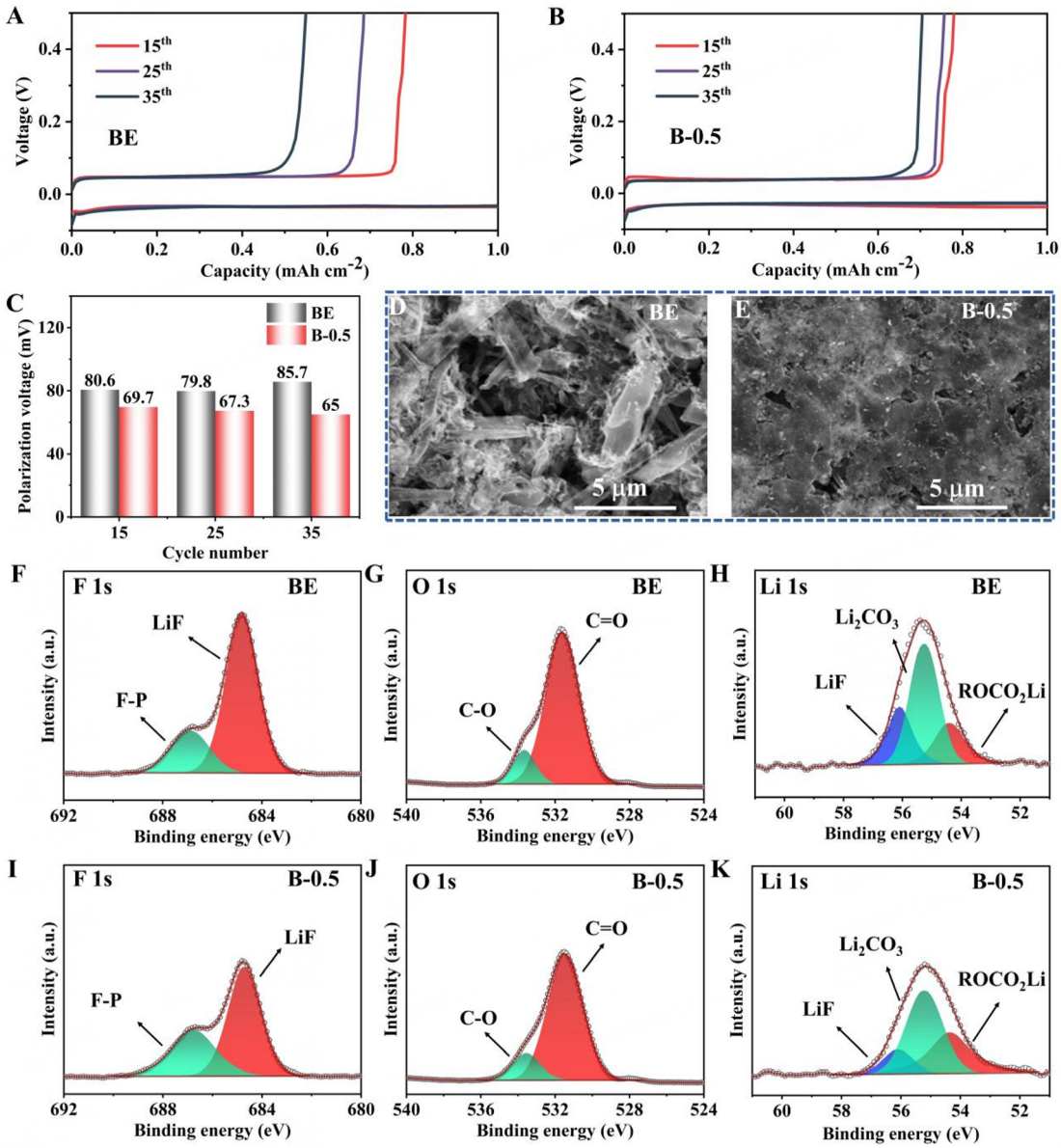

Figure 3. (A and B) Li plating/stripping voltage profiles with different electrolytes at the 15th, 25th and 35th cycles under the conditions of 1 mA cm^{-2} and 1 mAh cm^{-2}. (C) Polarization voltages at different cycles (0.3 mAh cm^{-2}). (D and E) Morphology of Li deposited on Cu substrate after ten cycles in Li||Cu cells with (D) BE and (E) B-0.5 at 1 mA cm^{-2}. (F-K) XPS spectra for Li||Li symmetric cells after ten cycles with (F-H) BE and (I-K) B-0.5.

using a B-0.5 electrolyte [Figure 3E]. The high ionic conductivity at the interface of the cell with B-0.5 would reduce the nucleation overpotential and enable the uniform deposition of lithium metal, thereby preventing the risk of short circuits[15].

After ten cycles of Li||Li symmetric cells with a current density of 1 mA cm^{-2} and a capacity of 1 mAh cm^{-2}, the SEI composition on the surface of Li electrodes is analyzed by XPS to gain a deeper understanding of how the additive B_2O_3 helps to regulate the plating morphology and improve the reaction kinetics. As shown in Figure 3F-K, in F 1s XPS spectra, the content of LiF derived from BE is higher than that from B-0.5, indicating that more lithium salts are decomposed. LiF has electronic insulating properties but poor

ionic conductivity[20]. An appropriate amount of LiF can prevent electron tunneling, minimize capacity loss, and inhibit electrolyte decomposition. Nevertheless, excessive LiF is not beneficial for enhancing the electrochemical performance[30,31]. The O 1s XPS spectra in B-0.5 exhibit a lower content of C=O species compared to that in BE, suggesting the reduced solvent decomposition with the additive. Besides, in Li 1s XPS spectra, the lower contents of LiF and Li_2CO_3 further confirm the fewer side reactions in B-0.5[32]. After adding B_2O_3, the components of B-F and Li-B-O species can be clearly observed in Supplementary Figure 6A[33]. These results suggest that the additive is involved in the reduction reaction on the anode surface, and the products constitute the important parts of the SEI. Furthermore, the formation of B-F species can remove HF and decrease the content of LiF. The higher bond energy of B-F also enhances the SEI stability[34,35]. Besides, the lower F and Li contents in the SEI layer indicate fewer parasitic reactions and less consumption of active Li in B-0.5 [Supplementary Figure 6B]. From the XPS results, it can be seen that the decomposition of lithium salts and organic solvents is suppressed in B-0.5, benefitting to form a stable SEI composed of B-containing species and less LiF, which can promote uniform and rapid Li deposition.

Electrochemical performance of Li||LRM cells

To identify the optimal additive amount, the electrochemical properties of the Li||LRM cells with the electrolytes containing various amounts of B_2O_3 were evaluated. As shown in Supplementary Figure 7, the Li||LRM cell with B-0.5 electrolyte (B-0.5-cell) exhibits the best performance in the voltage range of 2-4.8 V at 1 C. Therefore, the electrolyte with 0.5 wt% of B_2O_3 additive is used in the following part. As depicted in Figure 4A, the Li||LRM cell with BE (BE-cell) exhibits a capacity retention of only 73.7% after 200 cycles at 1 C within 2-4.8 V. In contrast, the B-0.5-cell delivers a higher capacity retention of 92.1% after 200 cycles, which is nearly 20% more than that of BE. Moreover, the discharge capacity is up to 221 mAh g^{-1} and the average CE is also higher, reaching 99.1% after 200 cycles by introducing B_2O_3 into the BE. However, the initial CE of the BE-cell is 86%, while the B-0.5-cell exhibits a low CE of < 70%, which can be attributed to the interface reaction involving the additive. Moreover, the charge/discharge curves shown in Figure 4B and C indicate more pronounced voltage degradation in the BE-cell, as further confirmed in Figure 4D. The addition of B_2O_3 promotes the formation of a stable and durable CEI layer on the cathode surface, helping to maintain the stability of the cathode material. Besides, the existence of the robust CEI layer avoids the direct contact between the cathode and electrolyte, which can suppress the decomposition of the electrolyte, reduce the generation of by-products and decrease the consumption of active Li during the repeated rupture/repair process of CEI in subsequent cycles. Consequently, the capacity attenuation is significantly alleviated during long-term cycling.

Furthermore, the leakage current and self-discharge behavior were tested to assess the high-voltage stability at 4.8 V. The results show that the introduction of B_2O_3 evidently reduces the leakage current after 100 cycles [Figure 4E]. In the self-discharge tests conducted after 50 and 100 cycles, the voltage of BE-cells drops below 3.3 V after five days, and below 2 V after ten days [Figure 4F and Supplementary Figure 8]. In comparison, the B-0.5-cells can maintain a slower trend of voltage drop. The smaller leakage current and lower self-discharge level reveal that the CEI derived from B-0.5 has better stability under high voltage and helps to reduce the side reactions.

In addition, the rate capability was conducted under different current densities, as shown in Figure 4G. The B-0.5-cell exhibits better rate performance, and the discharge capacities are 278, 257, 239, 217, 202, and 179 mAh g^{-1} at the current densities of 0.2, 0.5, 1, 2, 3, 5 C, respectively. The reversible capacity is also restored more effectively after returning to the small current of 0.2 C. Besides, a 3 C cycling experiment was carried out after the rate performance tests. Compared to BE, B-0.5-cell reflects higher cycling stability and a slower decay trend during long-term cycling [Supplementary Figure 9]. As illustrated in

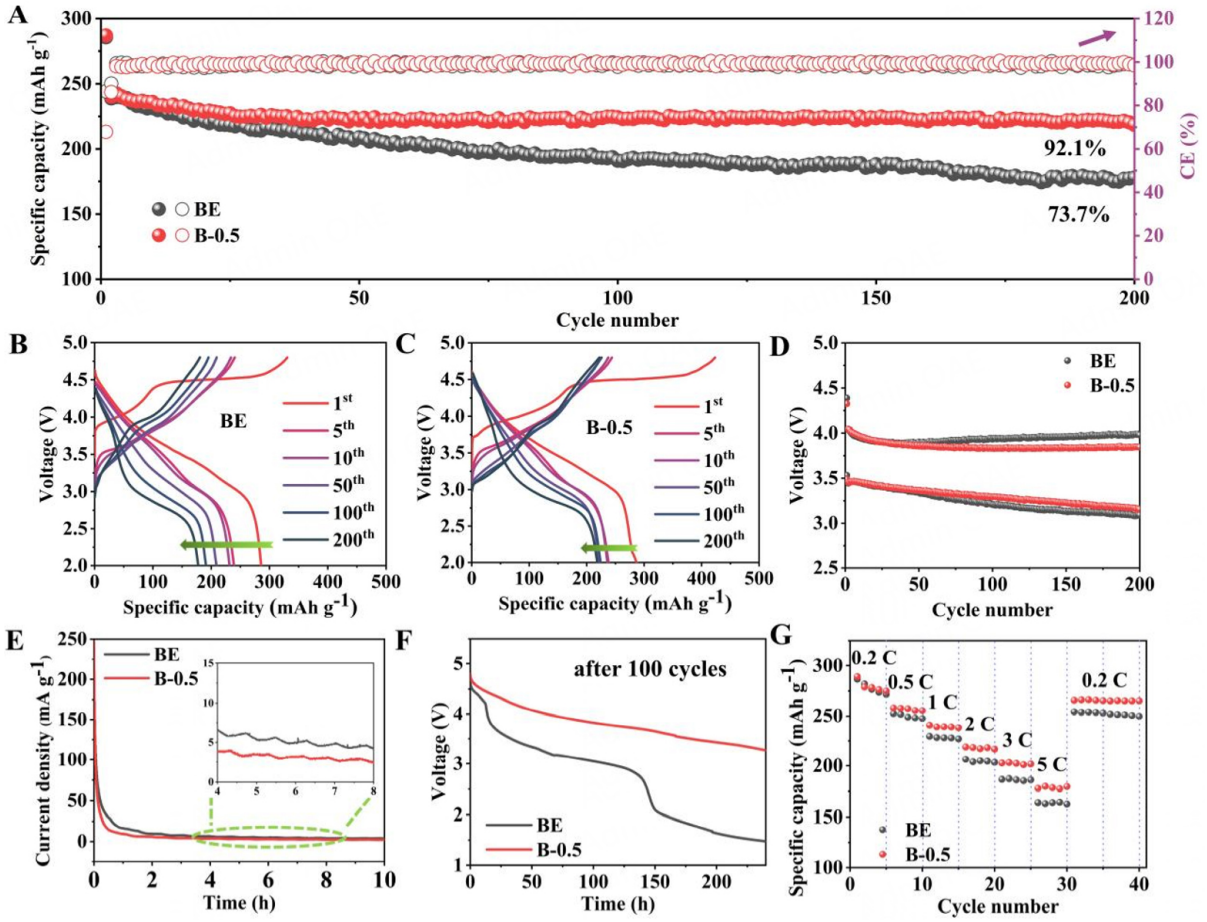

Figure 4. Electrochemical performances of Li||LRM cells in BE and B-0.5: (A) Cycling performance at 1 C. (B and C) Charge-discharge curves in (B) BE and (C) B-0.5. (D) Average charge/discharge voltage during cycling. (E) Leakage current during 4.8 V constant-voltage floating tests after 100 cycles. (F) Self-discharge curves after 100 cycles. (G) Rate performance.

Supplementary Figure 10, the capacity of BE-cell decreases to 91.7 mAh g^{-1} rapidly after 300 cycles when cycled at a high rate of 5 C, whereas a higher capacity of 154.7 mAh g^{-1} is sustained for B-0.5-cell under the same testing condition. The improvement can be attributed to the enhanced reaction kinetics of CEI in B-0.5-cell, which promotes rapid Li^+ transport and is also confirmed by the electrochemical impedance spectra (EIS) and GITT tests. As presented in Supplementary Figure 11, EIS was first employed to investigate the effect of the additive on the electrode/electrolyte interface. The semicircles in the high and middle-frequency regions are related to the film resistance (R_f) and charge transfer resistance (R_{ct}). The R_f in B-0.5-cell is slightly larger compared to that in BE-cell after five cycles, which may be linked to the formation of a protective layer by the additive [Supplementary Figure 11A][36]. After 100 cycles, the resistance in BE-cell increases more obviously, suggesting the decline in the interfacial conductivity [Supplementary Figure 11B]. The GITT tests reveal that the B-0.5-cell exhibits a higher D_{Li+} than the BE-cell during the charging and discharging process [Supplementary Figure 12].

The cycling performance under severe conditions is evaluated to comprehensively verify the effectiveness of the additive. The B-0.5-cell maintains a better cycling performance under a high mass loading of 12.1 mg cm^{-2} at 0.5 C, while the capacity of the BE-cell declines drastically after 15 cycles, as shown in Figure 5A. The stable CEI formed from B_2O_3-containing electrolyte not only protects the cathode structure,

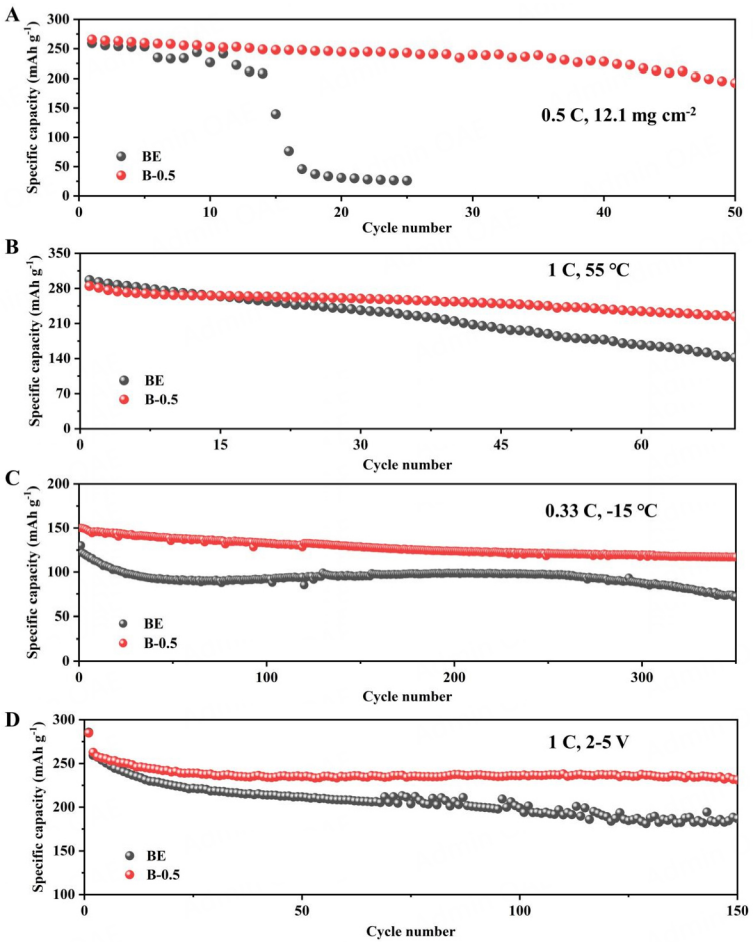

Figure 5. (A-C) Cycling performance in different electrolytes: (A) at 0.5 C with high mass loading of 12.1 mg cm^{-2}, (B) at 1 C and 55 °C, (C) at 0.33 C and -15 °C. (D) Cycling tests at 2-5 V under room temperature.

but also reduces side reactions, and the formed low-impedance interface layer also promotes interfacial Li^+ diffusion. Therefore, the cycling stability of the B-0.5-cell is significantly improved under high mass loading. In the high-temperature environment, the interfacial side reactions become more intense and the volume change is larger due to the deeper Li^+ deintercalation, while the increased polarization would lead to rapid attenuation of capacity and voltage at low temperature. This unfavorable low-temperature polarization is not only related to the increased electrolyte viscosity, but also to the compositions of the interface layer. The uniform and durable interface protective layer containing B components is obtained after introducing the additive into the electrolyte, which plays an important role in reducing the degree of electrolyte decomposition at high temperatures and improving the low-temperature kinetics. As a result, the B-0.5-cell delivers higher discharge capacity and mitigated voltage decay at 1 C and 55 °C [Figure 5B and Supplementary Figure 13]. Besides, under the testing conditions of 0.33 C and -15 °C, the discharge capacity of the B-0.5-cell remains at 117 mAh g^{-1} after 350 cycles with a capacity retention of 78%, which is higher than that of BE-cell (< 60%) [Figure 5C and Supplementary Figure 14]. As shown in Figure 5D and Supplementary Figure 15, increasing the upper cut-off voltage to 5 V, the B-0.5-cell achieves a discharge capacity of 233 mAh g^{-1} and a capacity retention of 88.8% after 150 cycles at 1 C, which are superior to BE-cell. The average CE of B-0.5-cell is as high as 98.8%, and the CE fluctuation is also obviously smaller than that of BE-cell [Supplementary Figure 16].

Morphological and structural changes of LRM cathode

For deep insights into the effect of the additive on stabilizing LRM cathodes under high voltage, the cycled cells were disassembled and evaluated. Upon cycling, the continuous decomposition of electrolyte will lead to the generation of HF, which corrodes the cathodes and damages the CEI film, ultimately resulting in the dissolution of TM. For the prepared LRM materials, the proportion of Mn is approximately four times higher than that of Ni and Co, and considering the possible testing errors, the content of Mn migrating to the anode can serve as a crucial indicator to reflect the dissolution degree of TM. In this context, the inductively coupled plasma (ICP) tests were performed to verify the content of Mn on the anode surface after cycling. Figure 6A shows that the content of the dissolved Mn element in B-0.5 is noticeably lower than that in BE. This result is attributed to the stable and durable CEI formed on the cathode surface and fewer harmful species including HF in B-0.5, thereby inhibiting the dissolution of TM and alleviating the structural degradation of LRM. In addition, the cathodes were tested by Raman spectroscopy to investigate the effect of the additive on phase change after 150 cycles. As depicted in Figure 6B, the vibrations near 495 and 600 cm^{-1} are attributed to the bending (E_g) and stretching (A_{1g}) modes of the layered structure, while the vibration at ~640 cm^{-1} corresponds to the characteristic peak of the spinel structure[37-39]. The larger blue shift of the A_{1g} peak indicates that more phase transitions have occurred in the LRM cathode from the BE-cell, which further reveals the beneficial effect of the additive in restraining the structural change of cathode material upon cycling.

The structural evolution of the LRM cathode in the first two cycles was also examined by *in-situ* XRD tests in Figure 6C and Supplementary Figure 17. Wherein, the angular variation of (003) diffraction peak is closely related to the intercalation/deintercalation behavior of Li^+ during the charging and discharging processes. In the early stage of charging, the extraction of Li^+ from the lithium layer causes an increase in the electrostatic repulsion between the oxygen layers, which results in the expansion of lithium layer spacing and the shift of (003) peak towards a low angle. As the voltage is gradually raised to around 4.5 V, Li^+ in the TM layer is extracted along with the activation of oxygen for charge compensation, and the (003) peak gradually moves back to the high-angle direction. Afterward, during the subsequent discharge stage, the extracted Li^+ is embedded back into the TM and lithium layers, corresponding to the movement of the (003) peak to the low and high angles, respectively. In the following cycles, the change of the (003) peak shows a similar trace as in the first cycle. Compared with the initial position, the (003) peak of the LRM cathode in B-0.5-cell shows a smaller average angle shift (0.175° and 0.185° in B-0.5 and BE), indicating the reduced volume change along the c-axis, which reveals the enhanced stability of the LRM cathode in B-0.5 electrolyte [Figure 6C][20]. Supplementary Figure 18 shows the XRD patterns of the initial LRM cathode and the cycled electrodes after 200 cycles in different electrolytes. The diffraction peaks of (003) and (104) in BE exhibit weaker signals, reflecting the more serious structural deterioration. Additionally, the (003) peak in BE also shows a more pronounced leftward shift, which can be ascribed to the higher consumption of active Li and larger polarization. The lack of active Li leads to an increased interlayer, resulting in a larger angle deviation.

To achieve an in-depth understanding of the enhanced electrochemical performance, the surface morphology of the LMA disassembled from the cycled Li||LRM cells is checked after 200 cycles. The morphology of the fresh LMA is tested by SEM and shown in Supplementary Figure 19. The whole surface is flat with slight streaky traces caused by mechanical processing. However, after long-term cycling, clearly different features are presented on the LMA surface in distinct electrolytes. Without an additive in BE, the anode surface appears to be distinctly black, with numerous mossy Li dendrites covered by side products [Figure 7A and B]. In contrast, the LMA in B-0.5 exhibits a cleaner, denser, and flatter surface due to the regulated SEI film [Figure 7C and D]. Moreover, the surface morphology of the LRM particles in B-0.5 is also cleaner and smoother after cycling compared with the rough and uneven surface of those in BE

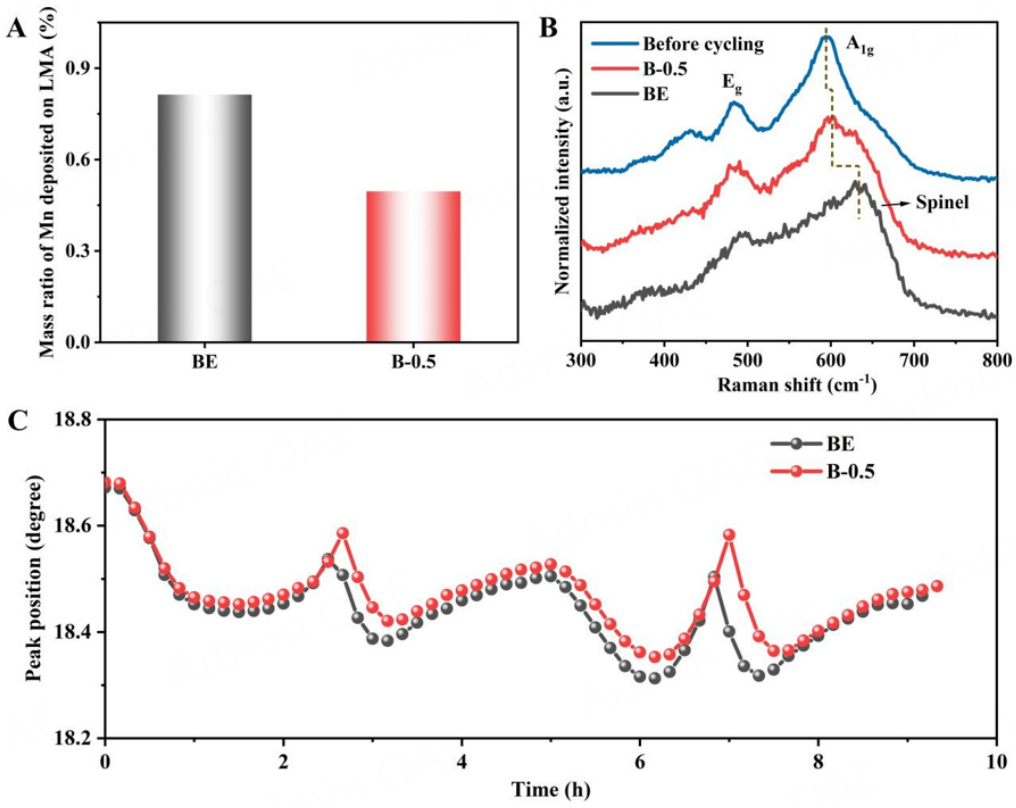

Figure 6. (A) The ICP test results of Mn element dissolved and deposited on LMA in BE-cell and B-0.5-cell after 200 cycles. (B) Raman spectra of the cathode material before and after cycling. (C) Variation of (003) peak during the initial two cycles by *in-situ* XRD tests.

[Figure 7E and F]. The TEM tests also reveal that a relatively uniform CEI layer with a thickness of 4-6 nm is formed on the cathode surface after cycling in B-0.5 [Supplementary Figure 20]. This protective CEI can maintain the stability of the cathode surface structure and suppress the electrolyte decomposition under high voltage, ultimately enhancing the long-term cycling performance.

The chemical composition of CEI on the cathode surface was identified by XPS [Figure 7G-L and Supplementary Figure 21]. The two peaks in F 1s XPS spectra correspond to LiF and C-F/P-F, and the stronger LiF signal indicates that more lithium salts are consumed in BE[31]. The O 1s XPS spectra contain three peaks, corresponding to C-O, C=O and TM-O. With the introduction of B_2O_3, the C-O peak is slightly stronger than that in BE, which is related to the products caused by the additive[25,40]. In P 2p XPS spectra, the two peaks represent $Li_xPO_yF_z$ and $PO4^{3-}$ species[31,41]. In the battery system, the substances containing F elements are PVDF and lithium salts, wherein PVDF has high chemical stability, which suggests that the generated F-containing species in the CEI mainly originates from the decomposition of lithium salts. From this perspective, the presence of higher LiF content with BE electrolyte illustrates that more lithium salt decomposition occurs [Figure 7G, J]. However, the content of P in BE is slightly lower than that in B-0.5 [Supplementary Figure 21B], indicating that some P-containing species derived from lithium salts in BE may be dissolved over cycling. The appearance of B-containing substances (such as Li-B-O, B_xO_y, and B-F) in B 1s XPS spectra directly demonstrates that B_2O_3 participates in the formation process of CEI [Supplementary Figure 21A][9,25]. These substances play a crucial role in reducing adverse reactions and enhancing the Li^+ diffusion rate[25,28]. Especially, the Li-B-O species can endow CEI with high mechanical and thermal stability[42]. The composition difference of CEI was further verified by TOF-SIMS. As depicted

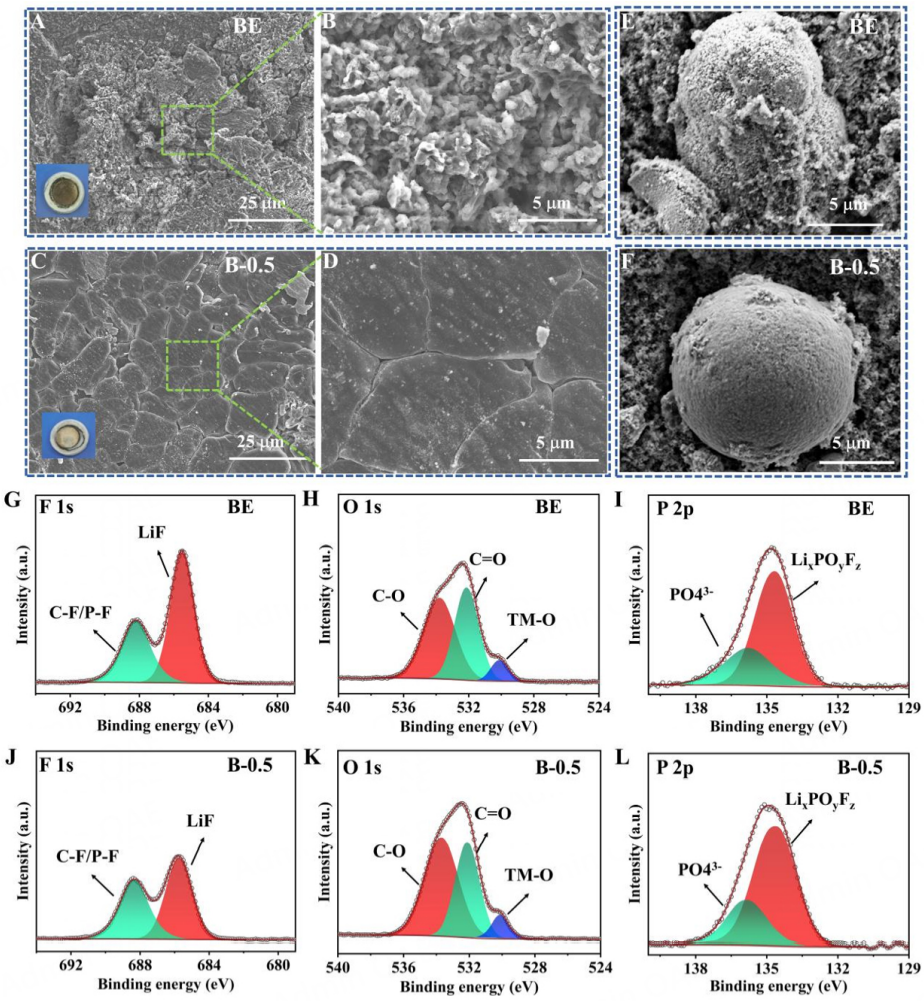

Figure 7. SEM images of LMAs disassembled from Li||LRM cells after 200 cycles with (A) BE and (C) B-0.5 electrolytes, wherein (B) and (D) are the corresponding locally enlarged images. SEM images of LRM particles after 200 cycles in (E) BE and (F) B-0.5 electrolytes. XPS spectra of the cycled LRM cathodes in (G-I) BE and (J-L) B-0.5 electrolytes.

in Supplementary Figure 22, the interface fragments contain more PO^- species in B-0.5, which is beneficial to elevating the CEI stability[43,44]. Besides, fewer MnF_3^- species demonstrate that the harmful reactions are suppressed in B-0.5, contributing to the integrity of CEI and cathode materials, which is consistent with the ICP results.

The improvement mechanism of the above proposed dual-functional electrolyte additive is schematically shown in Figure 8A and B, and summarized below: (I) The B_2O_3 additive can facilitate the formation of stable and durable SEI and CEI layers on the surface of cathodes and anodes. The regulated interface films can avoid the direct contact of electrode and electrolyte, thereby restraining the side reactions; (II) The generated B-F species can reduce the presence of HF; (III) The highly conductive SEI can suppress the Li dendrites growth; and (IV) The uniform and durable CEI can also stabilize the cathode structure and alleviate the dissolution of TM. These improvements ultimately enhance the electrochemical performance of cells.

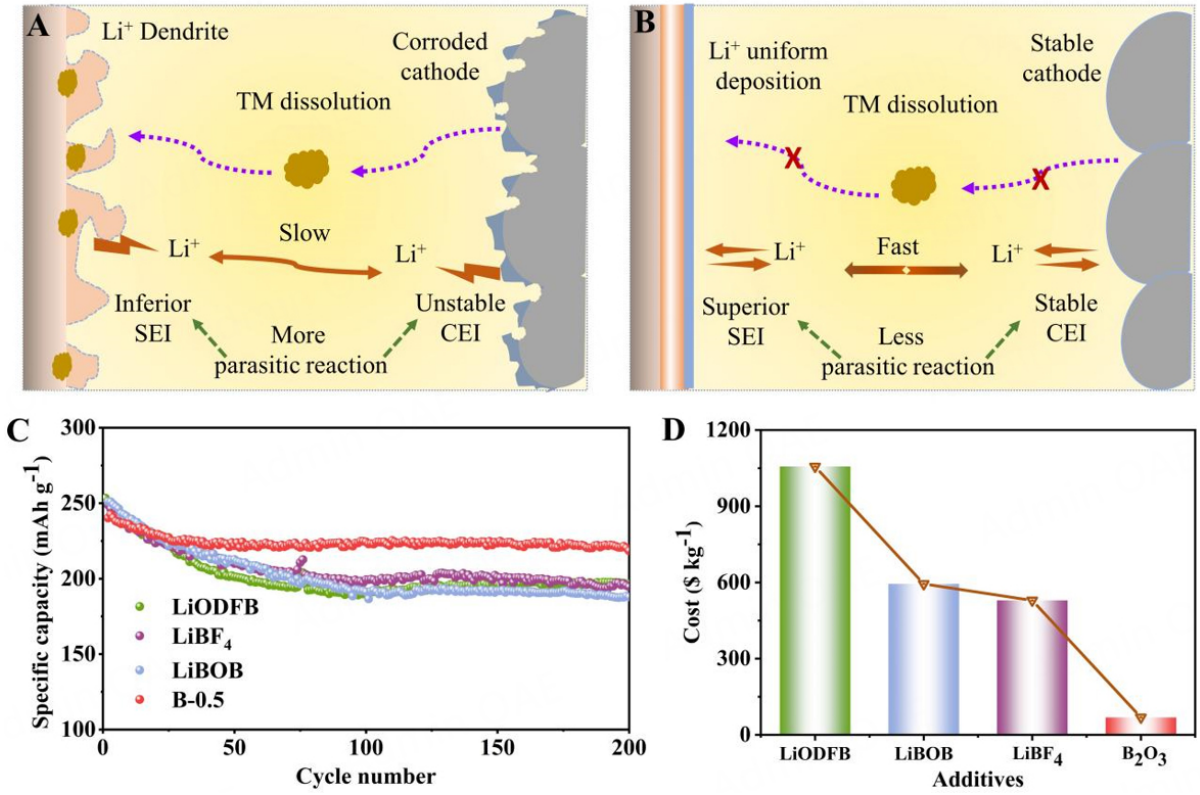

Figure 8. (A and B) Schematic illustrations of Li||LRM batteries using (A) BE and (B) B-0.5 electrolytes. (C) Cycling performance of Li||LRM batteries with 0.5 wt% different additives in the same electrolyte. (D) Cost comparison of different additives (Note: data from Manufacturer of Shanghai Aladdin Co., Ltd.).

Apart from the significant advance on improving performance, cost-effectiveness also needs to be considered for a good high-voltage additive. As depicted in Figure 8C, several conventional additives containing B were employed for the cycling tests in the voltage range of 2-4.8 V at 1 C. It is observed that, with the same amount of addition, the discharge capacity with B_2O_3 is evidently higher than other electrolytes after 200 cycles. Besides, the price of B_2O_3 is seven times lower than other additives [Figure 8D and Supplementary Table 1]. Its combined advantages of improved performance and low cost make it promising in commercial applications.

CONCLUSIONS

In summary, the inorganic oxide B_2O_3 is employed as a dual-functional additive in the carbonate electrolyte to enhance the performance of Li||LRM batteries by constructing durable CEI/SEI films. The B_2O_3 additive can participate in the interface reactions to form the functional protective layers containing B substances. The thin and uniform CEI formed on the cathode side can effectively maintain a stable layered structure of LRM with less TM dissolution and alleviate the continuous electrolyte decomposition. Moreover, the robust SEI formed on the LMA can regulate the deposition morphology with fewer dendrites, improve the CE during Li deposition and stripping process, and enhance the Li^+ transport kinetics. Hence, the enhanced cycling property is achieved. Specifically, the Li||LRM battery using the B_2O_3-containing electrolyte displays a high discharge capacity of 221 mAh g^{-1} after 200 cycles at 1 C with a high capacity retention of 92.1%. After increasing the upper cut-off voltage to 5 V, more than 85% capacity retention can still be obtained after 150 cycles at 1 C. This work proposes the use of low-cost inorganic oxide as a dual functional additive, providing an attractive new approach for the design and development of the high-voltage electrolyte.

DECLARATIONS

Authors' contributions

Conceptualization, methodology, formal analysis, investigation, data curation, writing - original draft: Zhou, D.

Investigation, formal analysis, validation, writing - review & editing: Gao, G.; Wei, G.; Guo, W.; Lin, L.; Zhang, C.; Li, S.; Liu, Y.

Visualization, writing - review & editing: Yang, Z.; Zhang, Y.; Sa, B.

Funding acquisition, project administration, resources, supervision, writing - review & editing: Peng, D. L.; Lin, J.; Xie, Q.

Availability of data and materials

The data supporting our findings can be found in the Supplementary Material.

Financial support and sponsorship

The work was supported by financial support from the National Natural Science Foundation of China (Grant Nos. 52272240, 51931006, U22A20118, and 52101273), Science and Technology Planning Projects of Fujian Province of China (Grant No. 2023H0003), the Fundamental Research Funds for the Central Universities of China (Xiamen University: Nos. 20720220074 and 20720240053), Science and Technology Projects of Innovation Laboratory for Sciences and Technologies of Energy Materials of Fujian Province (HRTP-[2022]-22) and the "Double-First Class" Foundation of Materials Intelligent Manufacturing Discipline of Xiamen University.

Conflicts of interest

All authors declared that there are no conflicts of interest.

Ethical approval and consent to participate

Not applicable.

Consent for publication

Not applicable.

REFERENCES

1. Jia, H.; Xu, W. Electrolytes for high-voltage lithium batteries. *Trends. Chem.* **2022**, *4*, 627-42. DOI
2. Ryu, H. H.; Park, K. J.; Yoon, C. S.; Sun, Y. K. Capacity fading of Ni-rich $Li[Ni_xCo_yMn_{1-x-y}]O_2$ ($0.6 \leq x \leq 0.95$) cathodes for high-energy-density lithium-ion batteries: bulk or surface degradation? *Chem. Mater.* **2018**, *30*, 1155-63. DOI
3. Lan, G.; Zhou, H.; Xing, L.; et al. Insight into the interaction between Ni-rich $LiNi_{0.8}Co_{0.1}Mn_{0.1}O_2$ cathode and BF_4^--introducing electrolyte at 4.5 V high voltage. *J. Energy. Chem.* **2019**, *39*, 235-43. DOI
4. Ko, S.; Obukata, T.; Shimada, T.; et al. Electrode potential influences the reversibility of lithium-metal anodes. *Nat. Energy.* **2022**, *7*, 1217-24. DOI
5. Xu, W.; Wang, J.; Ding, F.; et al. Lithium metal anodes for rechargeable batteries. *Energy. Environ. Sci.* **2014**, *7*, 513-37. DOI
6. Huang, Y.; Liu, X.; Yu, R.; et al. Tellurium surface doping to enhance the structural stability and electrochemical performance of layered Ni-rich cathodes. *ACS. Appl. Mater. Interfaces.* **2019**, *11*, 40022-33. DOI
7. Lee, W.; Muhammad, S.; Sergey, C.; et al. Advances in the cathode materials for lithium rechargeable batteries. *Angew. Chem. Int. Ed.* **2020**, *59*, 2578-605. DOI
8. Zheng, H.; Han, X.; Guo, W.; et al. Recent developments and challenges of Li-rich Mn-based cathode materials for high-energy lithium-ion batteries. *Mater. Today. Energy.* **2020**, *18*, 100518. DOI
9. Lu, Z.; Liu, D.; Dai, K.; et al. Tailoring solvation chemistry in carbonate electrolytes for all-climate, high-voltage lithium-rich batteries. *Energy. Storage. Mater.* **2023**, *57*, 316-25. DOI

10. Wu, H.; Dong, J.; Zhang, Y.; et al. Lattice oxygen redox reversibility modulation in enhancing the cycling stability of Li-rich cathode materials. *Adv. Funct. Mater.* **2023**, *33*, 2303707. DOI
11. Lee, H.; Nam, H.; Moon, J. H. Seamless integration of nanoscale crystalline-amorphous MoO_3 domains for high-performance lithium-sulfur batteries. *Energy. Storage. Mater.* **2024**, *70*, 103551. DOI
12. Su, H.; Chen, Z.; Li, M.; et al. Achieving practical high-energy-density lithium-metal batteries by a dual-anion regulated electrolyte. *Adv. Mater.* **2023**, *35*, e2301171. DOI
13. Han, J. G.; Lee, S. J.; Lee, J.; Kim, J. S.; Lee, K. T.; Choi, N. S. Tunable and robust phosphite-derived surface film to protect lithium-rich cathodes in lithium-ion batteries. *ACS. Appl. Mater. Interfaces.* **2015**, *7*, 8319-29. DOI
14. Zhao, H.; Lei, D.; He, Y. B.; et al. Compact 3D copper with uniform porous structure derived by electrochemical dealloying as dendrite-free lithium metal anode current collector. *Adv. Energy. Mater.* **2018**, *8*, 1800266. DOI
15. Yan, X.; Lin, L.; Han, X.; et al. Li dendrites inhibition realized by lithiophilic and ion/electron conductive 3D skeleton for Li metal anodes. *Chem. Eng. J.* **2021**, *421*, 127872. DOI
16. Um, K.; Jung, C.; Nam, H.; Lee, H.; Yeom, S.; Moon, J. H. Janus architecture host electrode for mitigating lithium-ion polarization in high-energy-density Li-S full cells. *Energy. Environ. Sci.* **2024**, *17*, 9112-21. DOI
17. Hu, A.; Chen, W.; Du, X.; et al. An artificial hybrid interphase for an ultrahigh-rate and practical lithium metal anode. *Energy. Environ. Sci.* **2021**, *14*, 4115-24. DOI
18. Xie, Y.; Huang, Y.; Zhang, Y.; et al. Surface modification using heptafluorobutyric acid to produce highly stable Li metal anodes. *Nat. Commun.* **2023**, *14*, 2883. DOI PubMed PMC
19. Zhu, Z.; Liu, Z.; Zhao, R.; et al. Heterogeneous nitride interface enabled by stepwise-reduction electrolyte design for dense Li deposition in carbonate electrolytes. *Adv. Funct. Mater.* **2022**, *32*, 2209384. DOI
20. Zheng, W. C.; Shi, C. G.; Dai, P.; et al. A functional electrolyte additive enabling robust interphases in high-voltage Li||$LiNi_{0.8}Co_{0.1}Mn_{0.1}O_2$ batteries at elevated temperatures. *J. Mater. Chem. A.* **2022**, *10*, 21912-22. DOI
21. Zhao, W.; Zheng, B.; Liu, H.; et al. Toward a durable solid electrolyte film on the electrodes for Li-ion batteries with high performance. *Nano. Energy.* **2019**, *63*, 103815. DOI
22. Gao, H.; Cai, J.; Xu, G. L.; et al. Surface modification for suppressing interfacial parasitic reactions of a nickel-rich lithium-ion cathode. *Chem. Mater.* **2019**, *31*, 2723-30. DOI
23. Liu, W.; Oh, P.; Liu, X.; et al. Nickel-rich layered lithium transition-metal oxide for high-energy lithium-ion batteries. *Angew. Chem. Int. Ed.* **2015**, *54*, 4440-57. DOI
24. Luo, C.; Liu, Q.; Wang, X.; et al. Synergistic-effect of diluent to reinforce anion-solvation-derived interfacial chemistry for 4.5 V-class Li||$LiCoO_2$ batteries. *Nano. Energy.* **2023**, *109*, 108323. DOI
25. Li, J.; Li, W.; You, Y.; Manthiram, A. Extending the service life of high-Ni layered oxides by tuning the electrode-electrolyte interphase. *Adv. Energy. Mater.* **2018**, *8*, 1801957. DOI
26. Xiao, Z.; Liu, J.; Fan, G.; et al. Lithium bis(oxalate)borate additive in the electrolyte to improve Li-rich layered oxide cathode materials. *Mater. Chem. Front.* **2020**, *4*, 1689-96. DOI
27. Zhao, Q.; Wu, Y.; Yang, Z.; et al. A fluorinated electrolyte stabilizing high-voltage graphite/NCM811 batteries with an inorganic-rich electrode-electrolyte interface. *Chem. Eng. J.* **2022**, *440*, 135939. DOI
28. Cheng, F.; Zhang, X.; Qiu, Y.; et al. Tailoring electrolyte to enable high-rate and super-stable Ni-rich NCM cathode materials for Li-ion batteries. *Nano. Energy.* **2021**, *88*, 106301. DOI
29. Shi, P.; Zhang, L.; Xiang, H.; Liang, X.; Sun, Y.; Xu, W. Lithium difluorophosphate as a dendrite-suppressing additive for lithium metal batteries. *ACS. Appl. Mater. Interfaces.* **2018**, *10*, 22201-9. DOI
30. Piao, Z.; Xiao, P.; Luo, R.; et al. Constructing a stable interface layer by tailoring solvation chemistry in carbonate electrolytes for high-performance lithium-metal batteries. *Adv. Mater.* **2022**, *34*, e2108400. DOI
31. Zhang, X.; Liu, G.; Zhou, K.; et al. Enhancing cycle life of nickel-rich $LiNi_{0.9}Co_{0.05}Mn_{0.05}O_2$ via a highly fluorinated electrolyte additive - pentafluoropyridine. *Energy. Mater.* **2022**, *1*, 100005. DOI
32. Wu, D.; He, J.; Liu, J.; et al. Li_2CO_3/LiF-rich heterostructured solid electrolyte interphase with superior lithiophilic and Li^+-transferred characteristics via adjusting electrolyte additives. *Adv. Energy. Mater.* **2022**, *12*, 2200337. DOI
33. Qin, Y.; Wang, D.; Liu, M.; et al. Improving the durability of lithium-metal anode via in situ constructed multilayer SEI. *ACS. Appl. Mater. Interfaces.* **2021**, *13*, 49445-52. DOI
34. Zhang, B.; Wang, L.; Wang, X.; et al. Sustained releasing superoxo scavenger for tailoring the electrode-electrolyte interface on Li-rich cathode. *Energy. Storage. Mater.* **2022**, *53*, 492-504. DOI
35. Li, Y.; Li, W.; Shimizu, R.; et al. Elucidating the effect of borate additive in high-voltage electrolyte for Li-rich layered oxide materials. *Adv. Energy. Mater.* **2022**, *12*, 2103033. DOI
36. Ye, C.; Tu, W.; Yin, L.; et al. Converting detrimental HF in electrolytes into a highly fluorinated interphase on cathodes. *J. Mater. Chem. A.* **2018**, *6*, 17642-52. DOI
37. Zheng, H.; Zhang, C.; Zhang, Y.; et al. Manipulating the local electronic structure in Li-rich layered cathode towards superior electrochemical performance. *Adv. Funct. Mater.* **2021**, *31*, 2100783. DOI
38. Li, S.; Liu, Y.; Zhang, Y.; et al. Interfacial oxygen coordination environment regulation towards high-performance Li-rich layered oxide cathode. *Chem. Eng. J.* **2023**, *462*, 142194. DOI
39. He, W.; Liu, P.; Qu, B.; et al. Uniform Na^+ doping-induced defects in Li- and Mn-rich cathodes for high-performance lithium-ion

batteries. *Adv. Sci.* **2019**, *6*, 1802114. DOI PubMed PMC

40. Ji, Y.; Li, S.; Zhong, G.; et al. Synergistic effects of suberonitrile-LiBOB binary additives on the electrochemical performance of high-voltage $LiCoO_2$ electrodes. *J. Electrochem. Soc.* **2015**, *162*, A7015. DOI
41. Xu, G.; Pang, C.; Chen, B.; et al. Prescribing functional additives for treating the poor performances of high-voltage (5 V-class) $LiNi_{0.5}Mn_{1.5}O_4$/MCMB Li-ion batteries. *Adv. Energy. Mater.* **2018**, *8*, 1701398. DOI
42. Wu, D.; Zhu, C.; Wang, H.; et al. Mechanically and thermally stable cathode electrolyte interphase enables high-temperature, high-voltage Li||$LiCoO_2$ batteries. *Angew. Chem. Int. Ed.* **2024**, *63*, e202315608. DOI
43. Fu, A.; Lin, J.; Zheng, J.; et al. Additive evolved stabilized dual electrode-electrolyte interphases propelling the high-voltage Li||$LiCoO_2$ batteries up to 4.7 V. *Nano. Energy.* **2024**, *119*, 109095. DOI
44. Zhao, J.; Zhang, X.; Liang, Y.; et al. Interphase engineering by electrolyte additives for lithium-rich layered oxides: advances and perspectives. *ACS. Energy. Lett.* **2021**, *6*, 2552-64. DOI